TRIPLE LONGITUDINAL FRACTURE OF INHOMOGENEOUS BEAM UNDER FOUR-POINT BENDING: AN ANALYTICAL STUDY BY USING A NON-LINEAR ELASTIC MATERIAL MODEL

Victor Rizov*

Department of Technical Mechanics, Faculty of Hydro-technique, University of Architecture, Civil Engineering and Geodesy, 1 Chr. Smirnesky blvd., 1046 - Sofia, Bulgaria

ARTICLE INFO

***Article history*:**
Received: 18.10.2022.
Received in revised form: 10.05.2023.
Accepted: 11.05.2023.

Keywords:
Continuously inhomogeneous beam
Longitudinal cracks
Non-linear elastic material

DOI: https://doi.org/10.30765/er.2052

Abstract:

The present paper is devoted to fracture analysis of an inhomogeneous non-linear elastic beam configuration with three parallel longitudinal cracks. The material is continuously inhomogeneous along the beam height. The beam is subjected to four-point bending. The longitudinal fracture behavior is studied by applying the J-integral approach. Solutions to the J-integral are obtained for the three cracks. For this purpose, the curvature and the coordinates of neutral axes of the crack arms are determined by using the equations for equilibrium of the elementary forces in the cross-sections of different portions of the beam. The solutions to the J-integral are valid for arbitrary locations of the cracks along the beam height. Thus, the solutions are very useful for evaluating of the effects of locations of cracks on the fracture. The longitudinal fracture behavior is studied also in terms of the strain energy release rate in order to verify the solutions to the J-integral. Solutions to the strain energy release rate are derived for the three cracks by considering the complementary strain energy in the beam. The solutions to the J-integral are applied to evaluate the effects of locations of the cracks, the material inhomogeneity, the sizes of the beam cross-section, and the coordinates of the applications points of the external forces on the longitudinal fracture behavior of the beam.

1 Introduction

Continuously (smoothly) inhomogeneous structural materials are nowadays widely used in various areas of engineering. These materials exhibit continuous variation of their properties along one or more coordinates in a structural member [1, 2, 3]. Thus, the material properties are continuous functions of one or more spatial coordinates. Among various kinds of continuously inhomogeneous structural materials, the functionally graded materials present a great deal of interest for practical engineering [4, 5, 6]. The functionally graded materials are relatively new inhomogeneous composites made of two or more constituent materials. Smooth variation of material properties of functionally graded material is obtained by gradually varying the composition of constituent materials during the manufacturing process. It should be mentioned that the macroscopic properties of the functionally graded materials can be formed technologically. The smooth variation of properties of functionally graded materials in one or more spatial coordinates can be tailored on order to achieve a better performance of the structural member to the external loads and influences. Thus, it is not surprising that the functionally graded materials have been used recently in more and more sophisticated

*Corresponding author.
E-mail address: v_rizov_fhe@uacg.bg

areas such as aerospace, aeronautics, nuclear power plants, robotics and biomedicine. Therefore, the mechanical reliability of the continuous inhomogeneous (functionally graded) structural members and components becomes increasingly important. In this relation, many authors have studied fracture in functionally graded structures [7, 8, 9, 10, 11]. These studies, however, usually deal with transversal or inclined cracks.

The significant interest in studying the mechanics of the longitudinal fracture of the continuously inhomogeneous beam structures is due to the fact that certain kinds of inhomogeneous materials such as the functionally graded materials can be built-up layer by layer [12, 13, 14] which favors appearance of longitudinal cracks between layers. These longitudinal cracks strongly influence the mechanical behavior and the integrity and reliability of the inhomogeneous beams. Besides, the longitudinal cracks may lead even to catastrophic failure of the entire structure. Thus, the operational performance of the inhomogeneous load-bearing engineering structures depends largely on their longitudinal fracture behavior. It should be noted that in the previous papers, the longitudinal fracture have been studied assuming presence of one longitudinal crack in the inhomogeneous beam [15, 16, 17, 18, 19, 20, 21]. However, the low transversal strength of inhomogeneous beam structures is a premise for appearance of more parallel longitudinal cracks between layers. Therefore, in contrast to [15, 16, 17, 18, 19, 20, 21], the present paper addresses the problem of longitudinal fracture by analyzing of an inhomogeneous four-point bending beam configuration with three parallel longitudinal cracks.

The tips of the three cracks are located in the middle portion of the beam that is under pure bending. The beam exhibits continuous material inhomogeneity along its height. The material has non-linear elastic behavior. The longitudinal fracture is studied by applying the *J*-integral approach. The longitudinal fracture behavior is analyzed also in terms of the strain energy release rate in order to verify the solutions of the *J*-integral for the three cracks obtained in the present paper. The strain energy release rate is derived by considering the complementary strain energy in the beam. The effects of various factors such as locations of the three cracks, material inhomogeneity, loading conditions and others on the longitudinal fracture behavior of the inhomogeneous non-linear elastic beam configuration are evaluated and discussed. The present paper may be regarded also as a contribution towards a better understating of peculiarities of the longitudinal fracture of continuously inhomogeneous non-linear elastic beams of layered structure.

1 Theoretical considerations

1.1 Calculation of the J-integral

An inhomogeneous beam with three parallel longitudinal cracks is shown in Figure 1. The beam is subjected to four-point bending by two vertical forces, F, applied at distance, l_1, from the ends of the beam. The length of the beam is l. The cross-section of the beam is a rectangle of width, b, and height, h. The three cracks are located arbitrary along the beam height. The heights of the cross-sections of crack arms 1, 2, 3 and 4 are denoted by h_1, h_2, h_3 and h_4, respectively. The tips of the three cracks are located in beam portion, H_1H_5. The beam is continuously inhomogeneous in the height direction.

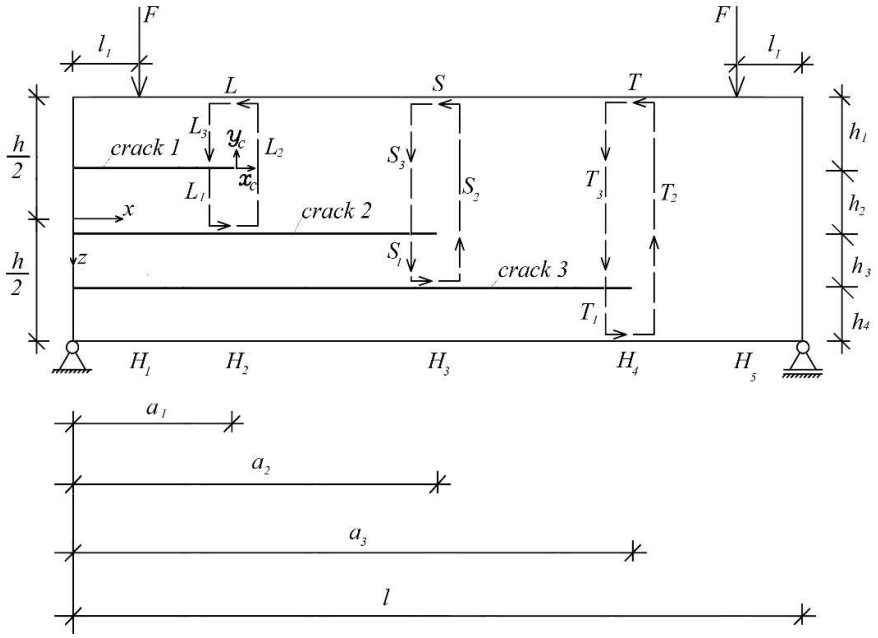

Figure 1. Geometry and loading of an inhomogeneous beam configuration with three longitudinal cracks.

Besides, the material of the beam has non-linear elastic mechanical behavior that is treated by applying the following stress-strain relation [22]:

$$\sigma = \frac{\varepsilon}{B + D\varepsilon}, \tag{1}$$

where σ is the stress, ε is the strain, B and D are material properties. The distribution of B along the beam height is written as

$$B = B_1 e^{m\frac{\frac{h}{2}+z}{h}}, \tag{2}$$

where

$$-\frac{h}{2} \le z \le \frac{h}{2}. \tag{3}$$

In (2), B_1 is the value of B in the upper surface of the beam, m is a material property that controls the material gradient along the height of the beam, the z -axis is shown in Fig. 1. It should be mentioned that at *m=0*, the beam is homogeneous. At *m>0* the beam is inhomogeneous. In this paper, we consider the case $m \ge 0$.

The longitudinal fracture behavior of the beam is analyzed by applying the *J*-integral approach [23]. First, crack 1 is considered. The *J*-integral is solved along the integration contour, *L*, shown by a dashed line in Figure 1. The solution of the *J*-integral is obtained as

$$J = J_{L_1} + J_{L_2} + J_{L_3}, \tag{4}$$

where J_{L_1}, J_{L_2} and J_{L_3} are the *J*-integral values in segments, L_1, L_2 and L_3, of the integration contour, respectively. The segments, L_1, L_2 and L_3, coincide with the cross-sections of crack arm 2, part, H_2H_3, of the beam (the boundaries of this part of the beam are $x=a_1$, $x=a_2$, $z=-h/2$ and $z=-h/2+h_1+h_2$) and crack arm 1, respectively.

In segment, L_1, the *J*-integral is written as

$$J_{L_1}=\int_{L_1}\left[u_{01}\cos\alpha-\left(p_{x_c}\frac{\partial u}{\partial x_c}+p_{y_c}\frac{\partial v}{\partial x_c}\right)\right]\mathrm{d}s\ , \tag{5}$$

where u_{01} is the strain energy density, α is the angle between the outwards normal vector to the contour of integration and the crack direction, p_x and p_y are the components of the stress vector, u and v are the components of the displacement vector and $\mathrm{d}s$ is a differential element along the contour of integration.

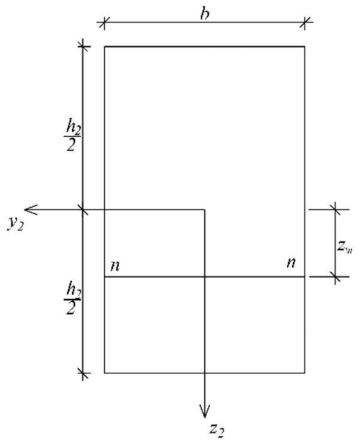

Figure 2. Cross-section of crack arm 2.

The components of (5) are found as

$$p_{x_c}=-\sigma\ , \tag{6}$$

$$p_{y_c}=0\ , \tag{7}$$

$$\mathrm{d}s=\mathrm{d}z_2\ , \tag{8}$$

$$\cos\alpha=-1\ , \tag{9}$$

$$\frac{\partial u}{\partial x_c}=\varepsilon \tag{10}$$

In (8), z_2 is the vertical centroidal axis of the cross-section of crack arm 2 (Figure 2). Thus,

$$-\frac{h_2}{2}\le z_2\le\frac{h_2}{2}\ . \tag{11}$$

The distribution of the strains that are involved in (10) is treated by applying the Bernoulli's hypothesis for plane sections because a beam of high span to height ratio is under consideration in the present paper. Hence, the distribution of strains in the cross-section of crack arm 2 is written as

$$\varepsilon = \kappa_1 \left(z_2 - z_{2n} \right), \tag{12}$$

where κ_1 is the curvature, z_{2n} is the coordinate of the neutral axis (Figure 2). It should be mentioned that the neutral axis, $n-n$, shifts from the centroid since the beam exhibits continuous material inhomogeneity in the height direction.

The curvature and the coordinate of neutral axis are determined in the following way. First, the equations for equilibrium of the elementary forces in the cross-section of crack arm 2 are written as

$$N_2 = \iint\limits_{(A_2)} \sigma \, \mathrm{d}A, \tag{13}$$

$$M_2 = \iint\limits_{(A_2)} \sigma \, z_2 \, \mathrm{d}A, \tag{14}$$

where N_2, M_2 and A_2 are the axial force, the bending moment and the area of the cross-section of this crack arm. From Figure 1, it follows that

$$N_2 = 0. \tag{15}$$

Equation (15) holds since we assume that there is no friction between the crack arms in the plane of each crack. As a result of this, the axial forces in the crack arms are zero.
In order to express the distribution of B in the cross-section of crack arm 2, formula (2) is re-written as

$$B = B_1 e^{m\frac{\frac{h_2}{2}+h_1+z_2}{h}}, \tag{16}$$

where

$$-\frac{h_2}{2} \le z_2 \le \frac{h_2}{2}. \tag{17}$$

By substituting of (1), (12), (15) and (16) in (13) and (14), one obtains

$$\begin{aligned} 0 = & -\frac{\kappa_1 z_{2n} b h_2}{B_1 e^f - D\kappa_1 z_{2n}} + \frac{\kappa_1 z_{2n} B_1 e^f g^2 b h_2^3}{24\left(B_1 e^f - D\kappa_1 z_{2n}\right)^2} - \\ & \frac{\kappa_1 \left(B_1 e^f g + D\kappa_1\right) b h_2^3}{12\left(B_1 e^f - D\kappa_1 z_{2n}\right)^2} - \frac{\kappa_1 z_{2n} \left(B_1 e^f g + D\kappa_1\right)^2 b h_2^3}{12\left(B_1 e^f - D\kappa_1 z_{2n}\right)^3}, \end{aligned} \tag{18}$$

$$M_2 = \frac{\kappa_1 b h_2^3}{12\left(B_1 e^{f} - D\kappa_1 z_{2n}\right)} + \frac{\kappa_1 z_{2n}\left(B_1 e^{f} g + D\kappa_1\right) b h_2^3}{12\left(B_1 e^{f} - D\kappa_1 z_{2n}\right)^2}. \tag{19}$$

where $f = \left(h_2/2 + h_1\right)m/h$, $g = m/h$. There are three un-known quantities (M_2, κ_1 and z_{2n}) in equations (18) and (19). Additional equations are composed by considering the equilibrium of the elementary forces in the cross-sections of the crack arms 1, 3 and 4 and by using the fact that the bending moment in the beam portion, H_1H_2, is distributed on the four crack arms. Besides, the four crack arms have the same curvature. Thus, by replacing of h_2 and z_{2n} with h_1 and the coordinate of neutral axis, z_{1n}, in (18) and (19), the equations for equilibrium of the elementary forces in the cross-section of crack arm 1 are written as

$$0 = -\frac{\kappa_1 z_{1n} b h_1}{B_1 e^{f_1} - D\kappa_1 z_{1n}} + \frac{\kappa_1 z_{1n} B_1 e^{f_1} g^2 b h_1^3}{24\left(B_1 e^{f_1} - D\kappa_1 z_{1n}\right)^2} - \frac{\kappa_1\left(B_1 e^{f_1} g + D\kappa_1\right) b h_1^3}{12\left(B_1 e^{f_1} - D\kappa_1 z_{1n}\right)^2} - \frac{\kappa_1 z_{1n}\left(B_1 e^{f_1} g + D\kappa_1\right)^2 b h_1^3}{12\left(B_1 e^{f_1} - D\kappa_1 z_{1n}\right)^3}, \tag{20}$$

$$M_1 = \frac{\kappa_1 b h_1^3}{12\left(B_1 e^{f_1} - D\kappa_1 z_{1n}\right)} + \frac{\kappa_1 z_{1n}\left(B_1 e^{f_1} g + D\kappa_1\right) b h_1^3}{12\left(B_1 e^{f_1} - D\kappa_1 z_{1n}\right)^2}, \tag{21}$$

where $f_1 = h_1 m/(2h)$. In (21), M_1 is the bending moment in crack arm 1, z_{1n} is the coordinate of the neutral axis of this crack arm.

Analogically, the equations for equilibrium of the elementary forces in the cross-sections of crack arms 3 and 4 are obtained as

$$0 = -\frac{\kappa_1 z_{3n} b h_3}{B_1 e^{f_2} - D\kappa_1 z_{3n}} + \frac{\kappa_1 z_{3n} B_1 e^{f_2} g^2 b h_3^3}{24\left(B_1 e^{f_2} - D\kappa_1 z_{3n}\right)^2} - \frac{\kappa_1\left(B_1 e^{f_2} g + D\kappa_1\right) b h_3^3}{12\left(B_1 e^{f_2} - D\kappa_1 z_{3n}\right)^2} - \frac{\kappa_1 z_{3n}\left(B_1 e^{f} g + D\kappa_1\right)^2 b h_3^3}{12\left(B_1 e^{f_2} - D\kappa_1 z_{3n}\right)^3}, \tag{22}$$

$$M_3 = \frac{\kappa_1 b h_3^3}{12\left(B_1 e^{f_2} - D\kappa_1 z_{3n}\right)} + \frac{\kappa_1 z_{3n}\left(B_1 e^{f_2} g + D\kappa_1\right) b h_3^3}{12\left(B_1 e^{f_2} - D\kappa_1 z_{3n}\right)^2}, \tag{23}$$

$$0 = -\frac{\kappa_1 z_{4n} b h_4}{B_1 e^{f_3} - D\kappa_1 z_{4n}} + \frac{\kappa_1 z_{4n} B_1 e^{f_3} g^2 b h_4^3}{24\left(B_1 e^{f_3} - D\kappa_1 z_{4n}\right)^2} - \frac{\kappa_1\left(B_1 e^{f_3} g + D\kappa_1\right) b h_4^3}{12\left(B_1 e^{f_3} - D\kappa_1 z_{4n}\right)^2} - \frac{\kappa_1 z_{4n}\left(B_1 e^{f_3} g + D\kappa_1\right)^2 b h_4^3}{12\left(B_1 e^{f_3} - D\kappa_1 z_{4n}\right)^3}, \tag{24}$$

$$M_4 = \frac{\kappa_1 b h_4^3}{12\left(B_1 e^{f_3} - D\kappa_1 z_{4n}\right)} + \frac{\kappa_1 z_{4n}\left(B_1 e^{f_3} g + D\kappa_1\right) b h_4^3}{12\left(B_1 e^{f_3} - D\kappa_1 z_{4n}\right)^2}, \tag{25}$$

where $f_2 = (h_3/2 + h_1 + h_2)m/h$, $f_3 = (h_4/2 + h_1 + h_2 + h_3)m/h$. The equation for equilibrium of the bending moments is written as (Figure 3)

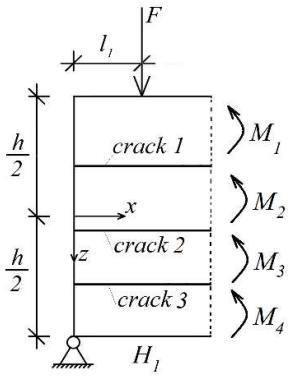

Figure 3. Bending moments in the four crack arms.

$$M = M_1 + M_2 + M_3 + M_4, \tag{26}$$

The bending moment, M, in the beam portion, H_1H_5, that is involved in (26) is found as (Figure 1)

$$M = Fl_1. \tag{27}$$

In (22) – (25), z_{3n} and z_{4n} are the coordinates of the neutral axes of cross-sections of crack arms 3 and 4, M_3 and M_4 are the bending moments in these crack arms. Equations (18) - (26) are solved with respect to κ_1, z_{1n}, z_{2n} z_{3n}, z_{4n}, M_1, M_2, M_3 and M_4 by using the MatLab computer program.

The strain distribution through the beam height for characteristic cross-sections is shown schematically in Figure 4. One can observe the schematic distribution of stresses in Figure 5.

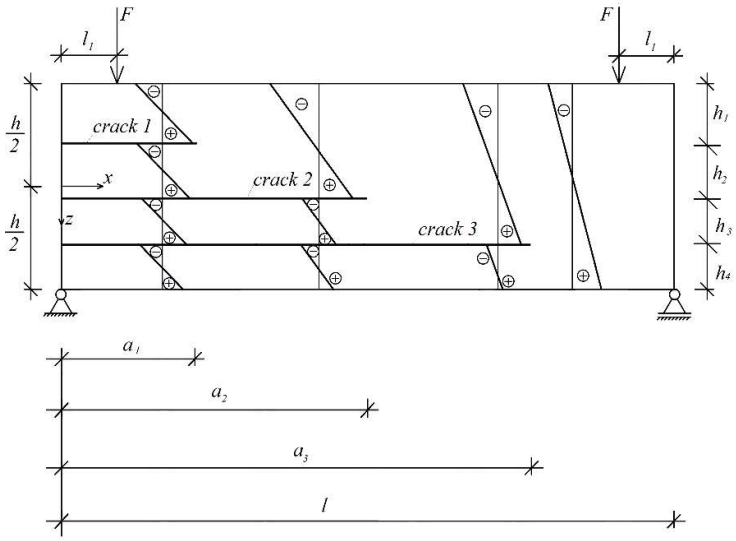

Figure 4. Schematic presentation of strain distribution through the beam height for characteristic cross-sections.

The strain energy density, u_{01}, that is involved in (5) is found by integrating of (1). The result is

$$u_{01} = \frac{1}{D}\left[\varepsilon - \frac{B}{D}\ln\left(\varepsilon + \frac{B}{D}\right) + \frac{B}{D}\ln\frac{B}{D}\right], \tag{28}$$

where ε is obtained by (12).
The *J*-integral in segment, L_2, of the integration contour is expressed as (Figure 1)

$$J_{L_2} = \int_{L_2}\left[u_{02}\cos\alpha_{L_2} - \left(p_{x_{L_2}}\frac{\partial u}{\partial x_{L_2}} + p_{y_{L_2}}\frac{\partial v}{\partial x_{L_2}}\right)\right]\mathrm{d}s_{L_2} \ . \tag{29}$$

The quantities which are involved in (29) are obtained as

$$p_{x_{L_2}} = \sigma_{L_2} . \tag{30}$$

Here the stress, σ_{L_2}, is found by replacing of ε with $\varepsilon_{H_2H_3}$ in the stress-strain relation (1) where $\varepsilon_{H_2H_3}$ is the strain in part, H_2H_3, of the beam.

$$p_{y_{L_2}} = 0, \tag{31}$$

$$\mathrm{d}s_{L_2} = -\mathrm{d}z_5 . \tag{32}$$

In formula (32), z_5 is the vertical centroidal axis of part, H_2H_3, of the beam. It is obvious that $-(h_1 + h_2)/2 \le z_5 \le (h_1 + h_2)/2$.

$$\cos\alpha_{L_2} = 1. \tag{33}$$

$$\frac{\partial u}{\partial x_{L_2}} = \varepsilon_{H_2H_3} . \tag{34}$$

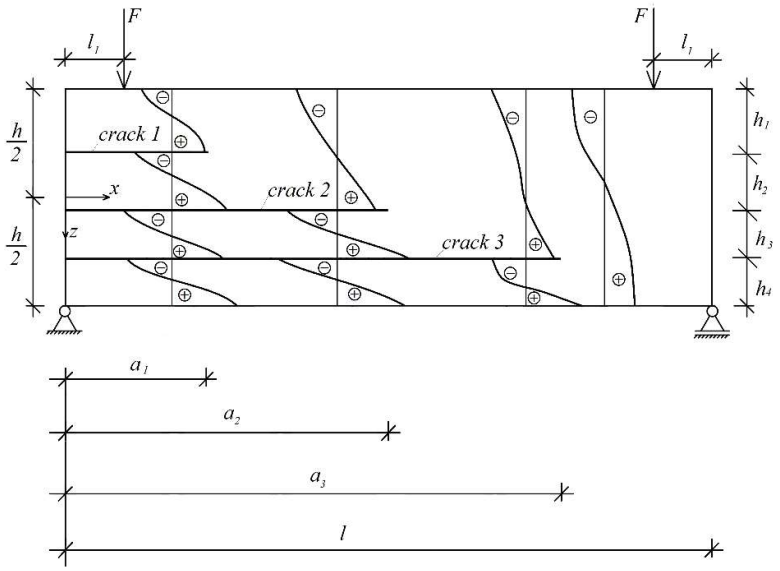

Figure 5. Schematic presentation of stresses distribution through the beam height for characteristic cross-sections.

The strain energy density, u_{02}, that is involved in (29) is found by (28). For this purpose, ε is replaced with $\varepsilon_{H_2H_3}$. The distribution of $\varepsilon_{H_2H_3}$ is obtained by replacing of κ_1, z_2 and z_{2n} with κ_2, z_5 and z_{5n} in (12). Here κ_2 is the curvature of the beam in portion, H_2H_3. The coordinate of the neutral axis is denoted by z_{5n}.

In order to determine the quantities, κ_2 and z_{5n}, first, the equations for equilibrium of the elementary forces in the cross-section of part, H_2H_3, of the beam are composed. For this purpose, M_2, κ_1, z_{2n} and h_2 are replaced, respectively, with $M_{1\delta}$, κ_2, z_{5n} and h_1+h_2 in (18) and (19) where $M_{1\delta}$ is the bending moment in part, H_2H_3, of the beam

$$0 = -\frac{\kappa_2 z_{5n} b\left(h_1+h_2\right)}{B_1 e^{f_4} - D\kappa_2 z_{5n}} + \frac{\kappa_2 z_{5n} B_1 e^{f_4} g^2 b h_2^3 \left(h_1+h_2\right)^3}{24\left(B_1 e^{f_4} - D\kappa_2 z_{5n}\right)^2} - \frac{\kappa_2\left(B_1 e^{f_4} g + D\kappa_2\right) b\left(h_1+h_2\right)^3}{12\left(B_1 e^{f_4} - D\kappa_2 z_{5n}\right)^2} - \frac{\kappa_2 z_{5n}\left(B_1 e^{f_4} g + D\kappa_2\right)^2 b\left(h_1+h_2\right)^3}{12\left(B_1 e^{f_4} - D\kappa_2 z_{5n}\right)^3}, \tag{35}$$

$$M_{1\delta} = \frac{\kappa_2 b\left(h_1+h_2\right)^3}{12\left(B_1 e^{f_4} - D\kappa_2 z_{5n}\right)} + \frac{\kappa_2 z_{6n}\left(B_1 e^{f_4} g + D\kappa_2\right) b\left(h_1+h_2\right)^3}{12\left(B_1 e^{f_4} - D\kappa_2 z_{5n}\right)^2}, \tag{36}$$

where $f_4 = \left(h_1+h_2\right)m/(2h)$. Further, by replacing of M_2, κ_1, z_{2n} and h_2 with $M_{2\delta}$, κ_2, z_{6n} and h_3 in (18) and (19), the equations for equilibrium of elementary forces in the cross-section of crack arm 3 in portion, H_2H_3, are written as

$$0 = -\frac{\kappa_2 z_{6n} b h_3}{B_1 e^{f_5} - D\kappa_2 z_{6n}} + \frac{\kappa_2 z_{6n} B_1 e^{f_5} g^2 b h_3^3}{24\left(B_1 e^{f_5} - D\kappa_2 z_{6n}\right)^2} - \frac{\kappa_2 \left(B_1 e^{f_5} g + D\kappa_2\right) b h_3^3}{12\left(B_1 e^{f_5} - D\kappa_2 z_{6n}\right)^2} - \frac{\kappa_2 z_{6n}\left(B_1 e^{f_5} g + D\kappa_2\right)^2 b h_3^3}{12\left(B_1 e^{f_5} - D\kappa_2 z_{6n}\right)^3}, \tag{37}$$

$$M_{2\delta} = \frac{\kappa_2 b h_3^3}{12\left(B_1 e^{f_5} - D\kappa_2 z_{6n}\right)} + \frac{\kappa_2 z_{6n}\left(B_1 e^{f_5} g + D\kappa_2\right) b h_3^3}{12\left(B_1 e^{f_5} - D\kappa_2 z_{6n}\right)^2}, \tag{38}$$

where $f_5 = \left(h_3/2 + h_1 + h_2\right) m/h$. In (37) and (38), $M_{2\delta}$ is the bending moment in crack arm 3 in portion, H_2H_3, z_{6n} is the coordinate of the neutral axis.

The equations for equilibrium of the elementary forces in the cross-section of crack arm 4 in portion, H_2H_3, are obtained by replacing of M_2, κ_1, z_{2n} and h_2 with $M_{3\delta}$, κ_2, z_{7n} and h_4 in (18) and (19)

$$0 = -\frac{\kappa_2 z_{7n} b h_4}{B_1 e^{f_6} - D\kappa_2 z_{7n}} + \frac{\kappa_2 z_{7n} B_1 e^{f_6} g^2 b h_4^3}{24\left(B_1 e^{f_6} - D\kappa_2 z_{7n}\right)^2} - \frac{\kappa_2 \left(B_1 e^{f_6} g + D\kappa_2\right) b h_4^3}{12\left(B_1 e^{f_6} - D\kappa_2 z_{7n}\right)^2} - \frac{\kappa_2 z_{7n}\left(B_1 e^{f_6} g + D\kappa_2\right)^2 b h_4^3}{12\left(B_1 e^{f_6} - D\kappa_2 z_{7n}\right)^3} \tag{39}$$

$$M_{3\delta} = \frac{\kappa_2 b h_4^3}{12\left(B_1 e^{f_6} - D\kappa_2 z_{7n}\right)} + \frac{\kappa_2 z_{7n}\left(B_1 e^{f_6} g + D\kappa_2\right) b h_4^3}{12\left(B_1 e^{f_6} - D\kappa_2 z_{7n}\right)^2}, \tag{40}$$

where $f_6 = \left(h_4/2 + h_1 + h_2 + h_3\right) m/h$. In (39) and (40), $M_{3\delta}$ and z_{7n} are the bending moment and the coordinate of neutral axis of crack arm 4 in portion, H_2H_3. The equation for equilibrium of the bending moments in beam portion, H_2H_3, is written as

$$M_{1\delta} + M_{2\delta} + M_{3\delta} = M. \tag{41}$$

Equations (35) – (41) are solved with respect to $M_{1\delta}$, $M_{2\delta}$, $M_{3\delta}$, κ_2, z_{5n}, z_{6n} and z_{7n} by using the MatLab computer program. The *J*-integral in segment, L_3, of the integration contour is written as

$$J_{L_3} = \int_{L_3}\left[u_{03}\cos\alpha_{L_3} - \left(p_{x_{L_3}}\frac{\partial u}{\partial x_{L_3}} + p_{y_{L_3}}\frac{\partial v}{\partial x_{L_3}}\right)\right] \mathrm{d}s_{L_3}, \tag{42}$$

where

$$P_{x_{L_3}} = -\sigma_{L_3}. \tag{43}$$

The stress, σ_{L_3}, is obtained by replacing of ε with $\varepsilon_{1\beta}$ in (1). The distribution of strain, $\varepsilon_{1\beta}$, in portion, H_1H_2, of crack arm 1 is derived by replacing of z_2 and z_{2n} with z_1 and z_{2n} in (12) where z_1 is the vertical centroidal axis of the cross-section of crack arm 1.

$$p_{y_{L_3}} = 0 . \tag{44}$$

$$\mathrm{d}s_{L_3} = \mathrm{d}z_1 , \tag{45}$$

where $-h_1/2 \le z_1 \le h_1/2$.

$$\cos\alpha_{L_3} = -1 . \tag{46}$$

$$\frac{\partial u}{\partial x_{L_3}} = \varepsilon_{1\beta} . \tag{47}$$

The strain energy density, u_{03}, that is involved in (42) is obtained by replacing of ε with $\varepsilon_{1\beta}$ in (28). By substituting of (5), (29) and (42) in (4), one arrives at

$$\begin{aligned} J = &\int_{L_1}\left[u_{01}\cos\alpha - \left(p_{x_c}\frac{\partial u}{\partial x_c} + p_{y_c}\frac{\partial v}{\partial x_c}\right)\right]\mathrm{d}s + \\ &+\int_{L_2}\left[u_{02}\cos\alpha_{L_2} - \left(p_{x_{L_2}}\frac{\partial u}{\partial x_{L_2}} + p_{y_{L_2}}\frac{\partial v}{\partial x_{L_2}}\right)\right]\mathrm{d}s_{L_2} + \\ &+\int_{L_3}\left[u_{03}\cos\alpha_{L_3} - \left(p_{x_{L_3}}\frac{\partial u}{\partial x_{L_3}} + p_{y_{L_3}}\frac{\partial v}{\partial x_{L_3}}\right)\right]\mathrm{d}s_{L_3} . \end{aligned} \tag{48}$$

The integration in (48) is performed by the MatLab computer program. The *J*-integral approach is applied also to investigate crack 2. The integration is carried-out along the integration contour, S, shown by a dashed line in Figure 1. Integration contour segments, S_1, S_2 and S_3, which coincide with the cross-sections of crack arm 3, part, H_3H_4, of the beam (the boundaries of this part of the beam are $x = a_2$, $x = a_3$, $z = -h/2$ and $z = -h/2 + h_1 + h_2 + h_3$) and part, H_2H_3, of the beam, respectively. The components of the *J*-integral in segments, S_1, S_2 and S_3, are found by using the corresponding expressions for components in segments, L_1, L_2 and L_3. For this aim, the following replacements are performed: p_{x_c}, p_{y_c}, $\mathrm{d}s$, $\cos\alpha$, $\partial u/\partial x_c$, $p_{x_{L_2}}$, $p_{y_{L_2}}$, $p_{y_{L_2}}$, $\mathrm{d}s_{L_2}$, $\cos\alpha_{L_2}$, $\partial u/\partial x_{L_2}$, $p_{y_{L_3}}$, $\mathrm{d}s_{L_3}$, $\cos\alpha_{L_3}$ and $\partial u/\partial x_{L_3}$ are replaced with σ_{S_1}, 0, $\mathrm{d}z_6$, -1, $\varepsilon_{1\delta}$, σ_{S_2}, 0, $-\mathrm{d}z_7$, 1, $\varepsilon_{H_3H_4}$, $-\sigma_{L_2}$, 0, $-\mathrm{d}z_5$, -1 and $\varepsilon_{H_2H_3}$, respectively. Here the vertical centroidal axis, z_6, of the cross-section of crack arm 3 varies in the interval $\left[-h_3/2; h_3/2\right]$. Besides, the vertical centroidal axis, z_8, of part, H_3H_4, of the beam varies in the interval $\left[\ -(h_1+h_2+h_3)/2; (h_1+h_2+h_3)/2\ \right]$.

The equation for equilibrium of the bending moments in the crack arms in portions, H_2H_3 and H_3H_4, of the beam are used when determining the curvatures and the coordinates of the neutral axes which are needed for the *J*-integral. The *J*-integral solution for crack 3 is derived along the integration contour with segments T_1, T_2 and T_3 (Figure 1) by performing replacements analogical to these described above for crack 2.

1.2 Verification

In order to verify the solutions to the *J*-integral, the fracture behavior of the beam is studied also in terms of the strain energy release rate, G. First, crack 1 is considered. The strain energy release rate is derived by applying the following differential dependence [15]:

$$G = \frac{\mathrm{d}U^*}{b\mathrm{d}a_1}, \tag{49}$$

where U^* is the complementary strain energy, $\mathrm{d}a_1$ is an elementary increase of crack 1. Only the complementary strain energy cumulated in beam portion, H_1H_5, is used when calculating the strain energy release rate by (49) since the tips of three cracks are located in this beam portion. Thus, the complementary strain energy is written as

$$U^* = U_1^* + U_2^* + U_3^* + U_4^* + U_5^* + U_6^* + U_7^*, \tag{50}$$

where U_1^*, U_2^*, U_3^*, U_4^*, U_5^*, U_6^* and U_7^* are the complementary strain energies cumulated in crack arm 1, crack arm 2, crack arm 3, crack 4, part, H_2H_3, of the beam, part, H_3H_4, of the beam and beam portion, H_4H_5, respectively.

The complementary strain energy in crack arm 1 is expressed as

$$U_1^* = (a_1 - l_1)\iint\limits_{(A_1)} u_{01}^* \mathrm{d}A, \tag{51}$$

where u_{01}^*, is the complementary strain energy density. The following dependence is applied to obtain u_{01}^* [16]:

$$u_{01}^* = \sigma\varepsilon - u_{01}. \tag{52}$$

By using of stress-strain relation (1) formula (52) is transformed as

$$u_{01}^* = \frac{\varepsilon^2}{B + D\varepsilon} - \frac{1}{D}\left[\varepsilon - \frac{B}{D}\ln\left(\varepsilon + \frac{B}{D}\right) + \frac{B}{D}\ln\frac{B}{D}\right]. \tag{53}$$

The complementary strain energy densities in other parts of the beam are derived by (53) by replacing of ε with the strain in the corresponding part of the beam. The complementary strain energies, U_2^*, U_3^*, U_4^*, U_5^*, U_6^* and U_7^*, are found by integrating of the corresponding complementary strain energy density.

By substituting of complementary strain energies in (49), one derives

$$G = \frac{1}{b}\left(\iint\limits_{(A_1)} u_{01}^* \mathrm{d}A + \iint\limits_{(A_3)} u_{03}^* \mathrm{d}A - \iint\limits_{(A_2)} u_{02}^* \mathrm{d}A \right). \tag{54}$$

The integration in (54) is performed by the MatLab computer program. It should be noted that the strain energy release rate obtained by (54) is match of the *J*-integral value found by (4). This fact is a verification of the

analysis of crack 1. Formula (54) is applied also to derive the strain energy release rate for cracks 2 and 3 after carrying-out the required replacements.
It should be mentioned that at $D = 0$, $1/B = E$ (here E is the modulus of elasticity of homogeneous material) and $m = 0$, the solutions of *J*-integral derived here transform in

$$J = \frac{18M^2}{Eb^2h^3}, \tag{55}$$

which is exact match of the solution of the strain energy release rate for homogeneous linear-elastic beam with a longitudinal crack in the mid-plane known from the literature [24]. This fact is an indication for correctness of the non-linear solutions since at $D = 0$, $1/B = E$ and $m = 0$ the non-linear stress-strain relation (1) transforms in the Hook's law.

2 Numerical results

The *J*-integral solutions are applied here in order to obtain numerical results which illustrate the effects of locations of cracks and the material inhomogeneity on the fracture behavior of the beam with three parallel longitudinal cracks. The *J*-integral value is presented in non-dimensional form by using the formula $J_N = JB_1/b$. The locations of cracks 1, 2 and 3 along the height of the beam are characterized by h_1/h, $(h_1 + h_2)/h$ and $(h_1 + h_2 + h_3)/h$ ratios, respectively. It is assumed that $b = 0.015$ m, $l = 0.400$ m and $D = 0.9B_1$.

In order to illustrate the effect of the location of crack 1 along the beam height on the longitudinal fracture behavior, the *J*-integral in non-dimensional form is plotted against h_1/h ratio in Figure 6 by using the *J*-integral solution (4) assuming that $(h_1 + h_2)/h = 0.6$ and $(h_1 + h_2 + h_3)/h = 0.8$.

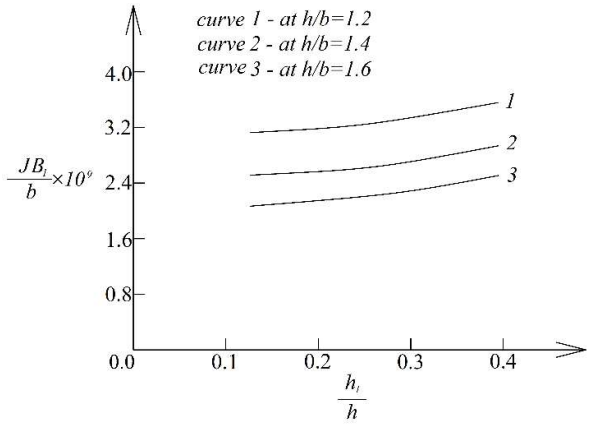

Figure 6. The J-integral value in non-dimensional form plotted against h_1/h ratio.

The effect of the sizes of the cross-section of the beam is illustrated also in Figure 6.

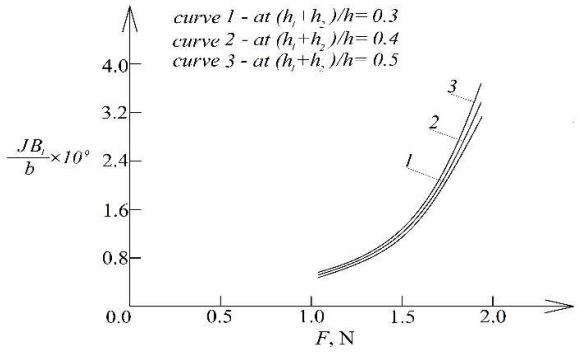

Figure 7. The J-integral value in non-dimensional form plotted against the external force, F .

For this purpose, three curves obtained at different h/b ratios are presented in Figure 6.

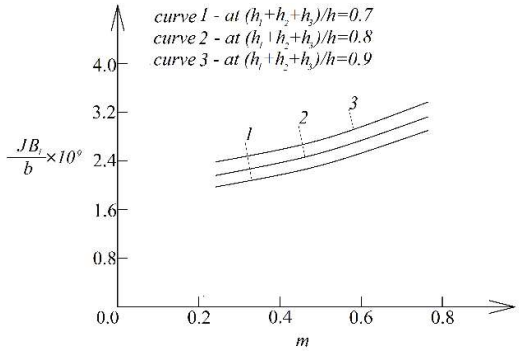

Figure 8. The J-integral value in non-dimensional form plotted against the material property, m .

One can observe in Figure 6 that the *J*-integral value increases with increasing of h_1/h ratio. It can also be observed in Figure 6 that the *J*-integral value decreases with increasing of h/b ratio.

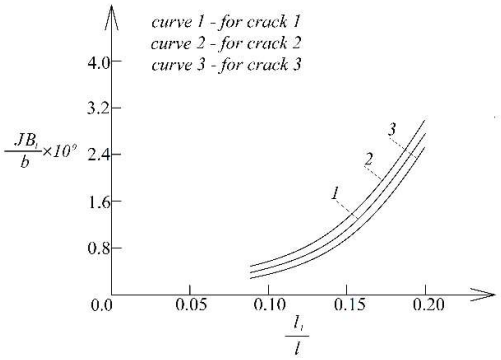

Figure 9. The J-integral value in non-dimensional form plotted against l_1/l ratio.

The influence of the location of crack 2 along the beam height on the longitudinal fracture is illustrated in Figure 7 where the *J*-integral value in non-dimensional form is plotted against the external force, F , at three $(h_1+h_2)/h$ ratios by applying the *J*-integral solution (73) assuming that $h_1/h=0.2$ and $(h_1+h_2+h_3)/h=0.7$. The curves in Figure 7 indicate that the *J*-integral value increases with increasing of $(h_1+h_2)/h$ ratio.

The influences of material inhomogeneity in the height direction and the location of crack 3 on the longitudinal fracture behavior of the beam are investigated too. For this purpose, the *J*-integral value in non-dimensional form is plotted against the material property, m, in Figure 8 at three values of $(h_1 + h_2 + h_3)/h$ ratio by using the *J*-integral solution (93) assuming that $h_1/h = 0.3$ and $(h_1 + h_2)/h = 0.5$. The curves in Figure 8 show that the *J*-integral value increases with increasing of $(h_1 + h_2 + h_3)/h$ ratio. One can observe also in Figure 8 that the *J*-integral value increases with increasing of m.

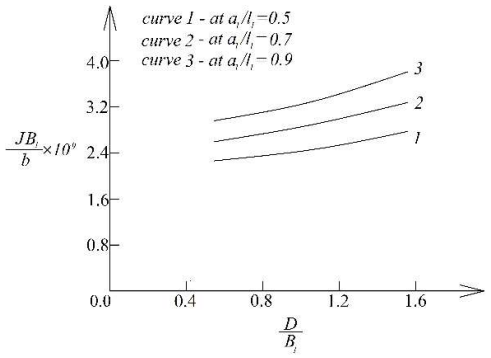

Figure 10. The J-integral value for crack 1 in non-dimensional form plotted against D/B_1 ratio.

The effect of the coordinates of the application points of the external forces on the longitudinal fracture behavior of the beam is illustrated in Figure 9 where the *J*-integral value in non-dimensional form is plotted against l_1/l ratio by using the *J*-integral solutions for the three cracks assuming that $h_1/h = 0.3$, $(h_1 + h_2)/h = 0.6$ and $(h_1 + h_2 + h_3)/h = 0.9$. It can be observed in Figure 9 that the *J*-integral value increases with increasing of l_1/l ratio. The curves in Figure 9 indicate that the *J*-integral value for crack 2 is higher than the *J*-integral values for cracks 1 and 3.

The *J*-integral value for crack 3 is lower than the *J*-integral values for cracks 1 and 2 (Figure 9). The *J*-integral value for crack 1 is intermediate with respect to the *J*-integral values for cracks 2 and 3. Concerning the influence of the length of cracks, it should be mentioned that when the tips of the cracks are located in the middle portion of the beam, the *J*-integral values do not depend on the crack length since the bending moment in the middle portion of the beam is constant. Therefore, in order to investigate the influence of the crack length, it is assumed that the tip of crack 1 is located in the first portion of the beam where the bending moment is found as $M = Fx_1$ (here $0 \le x_1 \le l_1$). The analysis indicates that when the tip of crack 1 is in the first portion of the beam, the *J*-integral value increases with increasing of the length of this crack (characterized by a_1/l_1 ratio) as shown in Figure 10.

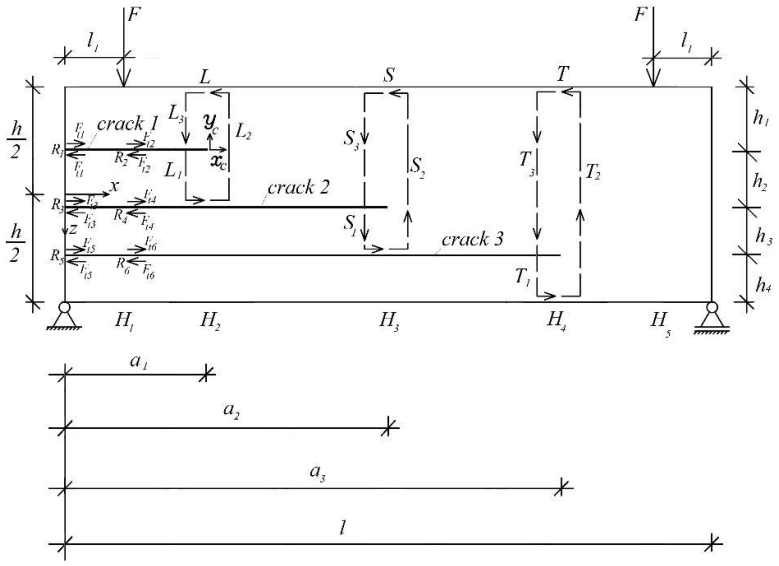

Figure. 11. Inhomogeneous beam configuration with friction forces, $F_{t1},F_{t2},...,F_{t6}$.

Finally, an analysis that takes into account the friction between the crack arms in the plane of each crack is developed. For this purpose, six friction forces, $F_{t1},F_{t2},...,F_{t6}$, between crack surfaces are introduced as shown in Figure 11. The friction forces are expressed as

$$F_{t1}=\mu F_1,\ F_{t2}=\mu F_2,\ F_{t3}=\mu F_3, \tag{56}$$

$$F_{t4}=\mu F_4,\ F_{t5}=\mu F_5,\ F_{t6}=\mu F_6, \tag{57}$$

where $F_1,F_2,...,F_6$ are the normal forces between crack surfaces in points $R_1,R_2,...,R_6$, μ is the coefficient of friction. Further, the equations of equilibrium of axial forces in the four crack arms are written as

$$N_1+F_{t1}+F_{t2}=0, \tag{58}$$

$$N_2-F_{t1}-F_{t2}+F_{t3}+F_{t4}=0, \tag{59}$$

$$N_3-F_{t3}+F_{t4}+F_{t5}+F_{t6}=0, \tag{60}$$

$$N_4-F_{t5}-F_{t6}=0, \tag{61}$$

where N_1, N_2, N_3 and N_4 are the axial forces in crack arms 1, 2, 3 and 4, respectively. The equations of equilibrium, $\sum V_i=0$, for crack arms 1, 2 and 3 are also used, i.e.

$$F_1+F_2-F=0, \tag{62}$$

$$-F_1-F_2+F_3+F_4=0, \tag{63}$$

$$-F_3-F_4+F_5+F_6=0. \tag{64}$$

From equations (56) – (64), it follows that

$$N_1 = -\mu F\,,\ N_2 = 0\,, \tag{65}$$

$$N_3 = 0\,,\ N_4 = \mu F\,. \tag{66}$$

The axial forces found by formulas (65) and (66) are substituted in the left-hand side of equilibrium equations (18), (20), (22) and (24). Thus, the left-hand side of equations (20) and (24) become $-\mu F$ and μF, respectively. Then equations (18) – (26) are solved with respect to κ_1, z_{1n}, z_{2n}, z_{3n}, z_{4n}, M_1, M_2, M_3 and M_4 by using the MatLab computer program. The left-hand sides of equilibrium equations (35) and (39) are also modified. They become $-\mu F$ and μF, respectively. Solution of the *J*-integral along the integration contour, *L*, is determined by (4).

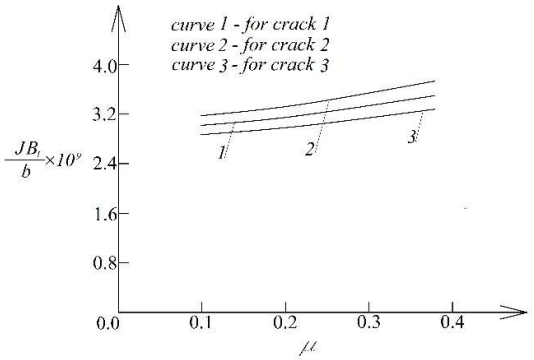

Figure 12. The J-integral value in non-dimensional form plotted against μ.

Similar procedure is applied to derive the solutions of the *J*-integral along the integration contours, *S* and *T*. These *J*-integral solutions are verified by applying the differential dependence (49) for determination of the strain energy release rate. The *J*-integral values are plotted versus μ in Figure 12 for the three cracks. One can observe that increase of μ generates increase of the *J*-integral value (Figure 12).

3 Conclusion

Fracture behavior of an inhomogeneous non-linear elastic beam with three parallel longitudinal cracks is analyzed by using the *J*-integral approach. The beam is loaded in four-point bending. The three cracks are located arbitrary along the beam height. The beam exhibits continuous material inhomogeneity in the height direction. Solutions to the *J*-integral are derived for the three cracks. The longitudinal fracture behavior is analyzed also in terms of the strain energy release rate for verification of the solutions to the *J*-integral. The effects of locations of the cracks along the beam height on the fracture are evaluated. The analysis reveals that the *J*-integral value increases with increasing of h_1/h, $(h_1+h_2)/h$ and $(h_1+h_2+h_3)/h$ ratios.

The effect of the sizes of the cross-section of the beam on the fracture behavior is evaluated too. It is found that the *J*-integral value decreases with increasing of h/b ratio. Concerning the effect of the material inhomogeneity on the fracture behavior, the investigation shows that the *J*-integral value increases with increasing of material property, m. The effect of the coordinates of the application points of the external forces on the fracture is also studied. It is found that the *J*-integral value increases with increasing of l_1/l ratio. It is found also that the *J*-integral value for crack 2 is higher than the *J*-integral values for cracks 1 and 3.

The lowest value has the *J*-integral for crack 3. The *J*-integral value for crack 1 is intermediate with respect to the *J*-integral values for cracks 2 and 3. The friction between the cracks arms is also considered. Thus, one of the essential novelties in the present paper is the fact that effects of three important factors (non-linear elastic behavior, continuous material inhomogeneity and friction between the arms of the longitudinal cracks) are taken into account. It should be mentioned that the present analysis can be developed further for different crack configurations with more than three parallel cracks. From practical viewpoint, the solutions derived can be applied to check for crack propagation. For this purpose, the *J*-integral values calculated by using the proposed solutions for the three cracks should be compared with corresponding individual critical values (i.e., the fracture resistance) of each crack in order to check whether cracks will start to propagate.

These corresponding individual critical values should be determined experimentally. However, there is a fracture resistance profile along the height of the beam due to the fact that the beam is inhomogeneous in the height direction. Therefore, fracture tests with initial longitudinal crack located at different positions along the beam height have to be carried-out.

References

[1] Tokovyy, Y., Ma, C.-C.: *Three-Dimensional Temperature and Thermal Stress Analysis of an Inhomogeneous Layer*, Journal of Thermal Stresses, 36(2013), 2, 790 - 808 DOI: 10.1080/01495739.2013.787853.

[2] Tokova, L., Yasinskyy, A., Ma, C.-C.: *Effect of the layer inhomogeneity on the distribution of stresses and displacements in an elastic multilayer cylinder*, Acta Mechanica, (2016), DOI: 10.1007/s00707-015-1519-8, 1 – 13.

[3] Tokovyy, Y., Ma, C.-C.: *Axisymmetric Stresses in an Elastic Radially Inhomogeneous Cylinder Under Length-Varying Loadings*, ASME Journal of Applied Mechanics, 83(2016): DOI: 10.1115/1.4034459.

[4] Hirai, T., Chen, L.: *Recent and prospective development of functionally graded materials in Japan*, Mater Sci. Forum, 308-311(1999), 2, 509-514.

[5] Suresh, S., Mortensen, A.: *Fundamentals of functionally graded materials*. IOM Communications Ltd, London, 1998.

[6] Nemat-Allal, M.M., Ata, M.H., Bayoumi, M.R. Khair-Eldeen, W.: *Powder metallurgical fabrication and microstructural investigations of Aluminum/Steel functionally graded material*, Materials Sciences and Applications, 2(2011), 2, 1708-1718.

[7] Upadhyay, A.K., Simha, K.R.Y.: *Equivalent homogeneous variable depth beams for cracked FGM beams; compliance approach*, Int. J. Fract., 144(2007), 209-213.

[8] Tilbrook, M.T., Moon, R.J., Hoffman, M.:*Crack propagation in graded composites*, Composite Science and Technology, 65(2005), 201-220.

[9] Carpinteri, A., Pugno, N.: *Cracks in re-entrant corners in functionally graded materials*, Engineering Fracture Mechanics, 73(2006), 1279-1291.

[10] Fett, T., Munz, D.: *A weight function for cracks in gradient materials*, Int. J. Fracture, 84(1997), L3-7.

[11] Karel Slámečka, David Jech, Lenka Klakurková, Serhii Tkachenko, Michaela Remešová, Pavel Gejdoš, Ladislav Čelko, Thermal cycling damage in pre-oxidized plasma-sprayed *M*CrAlY + YSZ thermal barrier coatings: Phenomenon of multiple parallel delamination of the TGO layer, Surface and Coatings Technology, 384, 2020, 125328.

[12] Miyamoto, Y., Kaysser, W.A., Rabin, B.H., Kawasaki, A., Ford, R.G.: *Functionally Graded Materials: Design, Processing and Applications*, Kluwer Academic Publishers, Dordrecht/London/Boston, 1999.

[13] Mahamood, R.M., Akinlabi, E.T.: *Functionally Graded Materials*, Springer, 2017.

[14] Bohidar, S.K., Sharma, R., Mishra, P.R.: *Functionally graded materials: A critical review*, International Journal of Research, 1(2014), 4, 289-301.

[15] Rizov, V.I.: *Analysis of longitudinal cracked two-dimensional functionally graded beams exhibiting material non-linearity*, Frattura ed Integrita Strutturale, 41(2017), 498-510.

[16] Rizov, V.I.: *Analysis of cylindrical delamination cracks in multilayered functionally graded nonlinear elastic circular shafts under combined loads*, Frattura ed Integrita Strutturale, 46(2018), 158-177.
[17] Rizov, V.I.: *Influence of material inhomogeneity and non-linear mechanical behavior of the material on delamination in multilayered beams*, Frattura ed Integrita Strutturale, 47(2019), 468-481.
[18] Rizov, V.I.: *Delamination of Multilayered Functionally Graded Beams with Material Nonlinearity*, International Journal of Structural Stability and Dynamics, (2018), doi.org/10.1142/S0219455418500517.
[19] Rizov, V.: *Lengthwise fracture analyses of functionally graded beams by the Ramberg-Osgood equation*, Engineering Review, 38(2018), 3, 309-320.
[20] Rizov, V.: *Analysis of delaminations in non-linear elastic multilayered inhomogeneous beam configurations*, Engineering Review, 40(2020), 3, 65-77.
[21] Rizov, V.: *Longitudinal fracture analysis of continuously inhomogeneous beam in torsion with stress relaxation*, Procedia Structural Integrity, 28(2020), 1212-1225.
[22] Rudih, O.L., Sokolov, G.P., Pahomov, V.L.: *Introduction to non-linear structural mechanics*. IASV, 1998.
[23] Broek, D.: *Elementary engineering fracture mechanics*. Springer, 1986.
[24] Hutchinson, J.W., Suo, Z.: *Mixed mode cracking in layered materials*, Adv. Appl. Mech., 64(1992), 804 – 810.